American Journal of Botany

RESEARCH ARTICLE

Early Miocene CO_2 estimates from a Neotropical fossil leaf assemblage exceed 400 ppm

Liliana Londoño[1,2,8], Dana L. Royer[3], Carlos Jaramillo[1], Jaime Escobar[1,4], David A. Foster[5], Andrés L. Cárdenas-Rozo[6], and Aaron Wood[7]

Manuscript received 2 April 2018; revision accepted 20 August 2018.

[1] Smithsonian Tropical Research Institute, Box 0843-03092, Balboa, Ancón, Republic of Panamá

[2] Departamento de Ciencias Ecológicas, Universidad de Chile, Santiago, Chile

[3] Department of Earth and Environmental Sciences, Wesleyan University, Middletown, Connecticut 06459, USA

[4] Departamento de Ingeniería Civil y Ambiental, Universidad del Norte, Barranquilla, Colombia

[5] Department of Geological Sciences, University of Florida, 241 Williamson Hall, Gainesville, Florida 32611, USA

[6] Departamento de Ciencias de la Tierra, Universidad EAFIT, Medellín, Colombia

[7] Department of Geological & Atmospheric Sciences, Iowa State University, Ames, Iowa, USA

[8] Author for correspondence (e-mail: liliana.londono@ug.uchile.cl)

Citation: Londoño, L., D. L. Royer, C. Jaramillo, J. Escobar, D. A. Foster, A. L. Cárdenas-Rozo, and A. Wood. 2018. Early Miocene CO_2 estimates from a Neotropical fossil leaf assemblage exceed 400 ppm. *American Journal of Botany* 105(11): 1–9.

doi:10.1002/ajb2.1187

PREMISE OF THE STUDY: The global climate during the early Miocene was warmer than the present and preceded the even warmer middle Miocene climatic optimum. The paleo-CO_2 records for this interval suggest paradoxically low concentrations (<450 ppm) that are difficult to reconcile with a warmer-than-present global climate.

METHODS: In this study, we use a leaf gas-exchange model to estimate CO_2 concentrations using stomatal characteristics of fossil leaves from a late early Miocene Neotropical assemblage from Panama that we date to 18.01 ± 0.17 Ma via $^{238}U/^{206}Pb$ zircon geochronology. We first validated the model for Neotropical environments by estimating CO_2 from canopy leaves of 21 extant species in a natural Panamanian forest and from leaves of seven Neotropical species in greenhouse experiments at 400 and 700 ppm.

KEY RESULTS: The results showed that the most probable combined CO_2 estimate from the natural forests and 400 ppm experiments is 475 ppm, and for the 700 ppm experiments is 665 ppm. CO_2 estimates from the five fossil species exhibit bimodality, with two species most consistent with a low mode (528 ppm) and three with a high mode (912 ppm).

CONCLUSIONS: Despite uncertainties, it is very likely (at >95% confidence) that CO_2 during the late early Miocene exceeded 400 ppm. These results revise upwards the likely CO_2 concentration at this time, more in keeping with a CO_2-forced greenhouse climate.

KEY WORDS leaf gas-exchange model; stomata; fossil; Miocene; CO_2.

The early and middle Miocene (~23–12 Ma) is marked by abrupt changes in global mean surface temperature (Hansen et al., 2013) but considerable uncertainty in atmospheric CO_2 concentration (Beerling and Royer, 2011; see Fig. 1). This uncertainty stems from two sources: there are comparatively few CO_2 records during the early Miocene and, while sampling is better during the middle Miocene, estimates range between ~300 and 600 ppm.

The middle Miocene climatic optimum (MMCO, ~17–14 Ma) is a well-characterized period of relative warmth, with global mean surface temperatures likely increasing relative to the early Miocene by 2–3°C (Fig. 1A; Hansen et al., 2013). Existing CO_2 records suggest baseline concentrations <450 ppm just before and after the MMCO, with concentrations increasing by 100–400 ppm during the interval itself (Fig. 1B; Royer, 2014). Some recent records suggest >500 ppm CO_2 at the very beginning (23.0-21.7 Ma; Reichgelt et al., 2016; Tesfamichael et al., 2017) and towards the end of the Miocene (11–9 Ma; Mejía et al., 2017). In general, though, the juxtaposition of a considerably warmer climate during the Miocene with only moderate increases in CO_2 has proved challenging for climate modelers to simulate (Knorr et al., 2011; Bradshaw et al., 2015).

Here we provide constraints on CO_2 levels prior to the MMCO during the late early Miocene by analyzing the stomatal characteristics of fossil leaves from a locality in the Panama Canal basin. These CO_2 estimates expand our existing CO_2 record and provide a temporal context for understanding the MMCO that followed. We estimate CO_2 with the leaf gas-exchange model of Franks et al. (2014). This CO_2 proxy improves on methods that rely on univariate empirical calibrations between CO_2 and stomatal frequency (e.g., stomatal density or stomatal index) in several respects: it is driven by a mechanistic understanding of leaf photosynthesis, produces well-bounded CO_2 estimates even at high estimated CO_2, and is not limited to fossil taxa that are still living today (Franks et al., 2014).

To date, the Franks model has been tested on nine temperate species with either open-grown individuals or with CO_2-manipulation experiments inside growth chambers (Franks et al., 2014; Maxbauer et al., 2014; Barclay and Wing, 2016). The model has not yet been

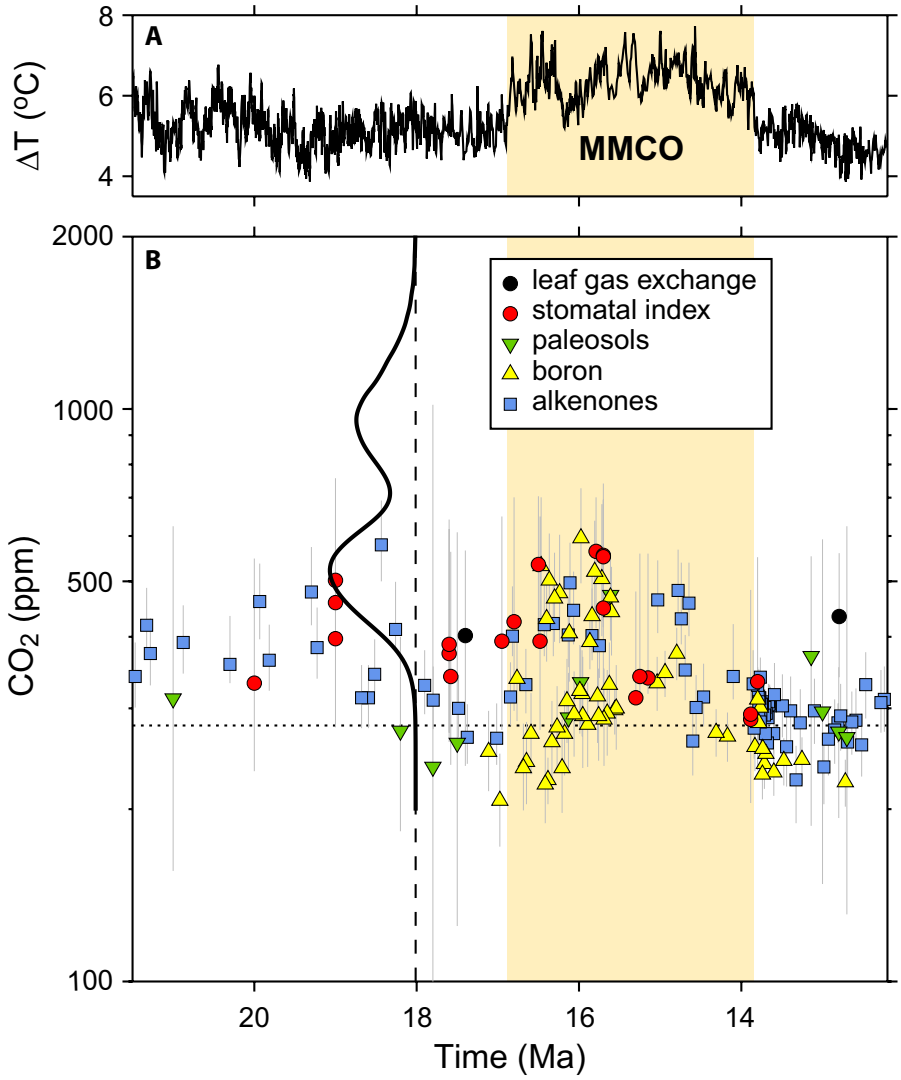

FIGURE 1. Miocene estimations of atmospheric CO_2 concentration and temperature. (A) Global mean surface temperature derived by Hansen et al. (2013) from the $\delta^{18}O$ compilation of benthic foraminifera by Zachos et al. (2008). MMCO = middle Miocene climatic optimum. (B) Proxy data of atmospheric CO_2 from stomata: Kürschner et al. (2008, 2008) [updated by Beerling et al. (2009)]; Royer et al. (2001) [updated by Beerling et al. (2009)]; Wang et al. (2015); Steinthorsdottir et al. (2018); leaf gas exchange: Grein et al. (2013) [updates Roth-Nebelsick et al. (2004)]; Franks et al. (2014); boron: Foster et al. (2012); Badger et al. (2013b); Greenop et al. (2014); paleosols: Quade and Cerling (1995) [reported in Ekart et al. (1999)]; Ekart et al. (1999); Retallack (2009) [updated by Breecker and Retallack (2014)]; Breecker and Retallack (2014); and alkenones: Zhang et al. (2013); Badger et al. (2013a); Super et al. (2018). Thin gray lines are the 95% confidence intervals for the proxy estimates. Black solid line is the probability density function of our CO_2 estimates from the Pedro Miguel fossil leaves (identical to Fig. 4C). Dashed horizontal line is the pre-industrial CO_2 (280 ppm).

tested on mature individuals in natural forest settings or on any species with Neotropical lineages; furthermore, only one species has been tested at elevated CO_2 (the conifer *Wollemia nobilis*). Thus, before applying the Franks model to our fossil species, we sought to validate the model with measurements from canopy leaves of 21 species growing in a natural Panamanian forest and from leaves of seven Neotropical species growing in CO_2-manipulated atmospheres of 400 and 700 ppm.

MATERIALS AND METHODS

Lithostratigraphic setting and depositional context

The angiosperm-bearing tuffaceous conglomerate is exposed in a fault-bound stratigraphic section within the Pedro Miguel Formation, Panama Canal basin (9.0047°N, 79.6051°W; Fig. 2). This formation is characterized by rocks formed by pyroclastic and lava deposits from the early Miocene (Montes et al., 2012; MacFadden et al., 2014).

The base of lithological unit 1 is a 0.8 meter-thick mudstone that grades in color from yellowish brown to olive gray at its top and exhibits weakly-defined horizontal bedding, abundant pedogenic slickensides, rhizohaloes, and millimeter-scale rounded fragments of lignite and volcaniclastic pebbles. The mudstone has an erosional overlying contact with a stack of three tuffaceous siltstones: each are less than a meter thick, fining upwards, contain weak horizontal bedding, exhibit organic-rich mudstones at their tops, and are separated by erosional contacts. The thickest of the three tuffaceous siltstones appears to consist of amalgamated lenticular bedforms and exhibits rare rhizoliths and carbonized plant debris. The uppermost 1.5 meters of lithological unit 1 preserves a stack of 20- to 50-cm-thick fining upwards sequences of pyroclastic material, separated by erosional contacts. The base of each sequence consists of very fine lithic sand supporting subangular lapilli that occasionally exceed a centimeter in diameter (Fig. 3A). The sequences grade into predominately silt-sized material and are capped by 0.5- to 1-cm-thick, organic-rich mudstones with rare horizontal trace fossils. Occasionally, the organic-rich mudstone of an underlying sequence is separated from the overlying very fine lithic sand by a cm-thick white volcanic ash. The thickest fining upwards sequence (~50 cm) exhibits trough cross-bedding and low-angle planar cross-bedding. This unit is interpreted as a succession of subaerial resedimented volcaniclastic mass flow deposits, the first of which was exposed long enough for development of an immature paleosol. The amalgamated lenticular bedforms in the tuffaceous siltstones may have been produced by erosive overland flows whereas the fining upwards sequence with trough and low-angle planar cross-bedding may represent the only subaqueous (fluvial) volcaniclastic debris flow in the unit. The overlying contact with lithological unit 2 is sharp and planar.

The 1.8-m-thick bluish gray claystone of lithological unit 2 exhibits extensive slickensides with red staining and yellowish brown rhizohaloes throughout. The bluish gray claystone of this unit is

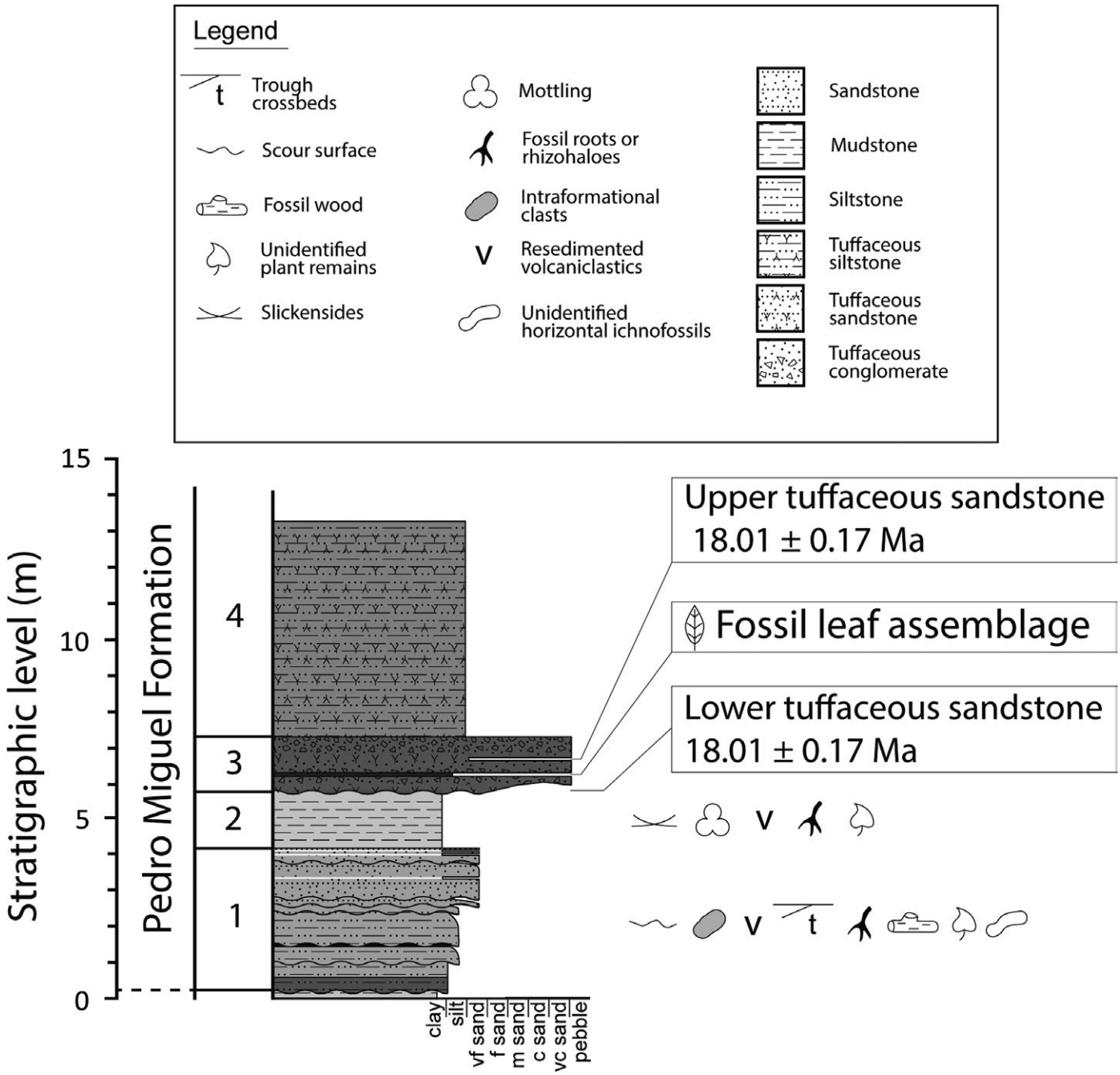

FIGURE 2. Lithostratigraphic section encompassing the early Miocene angiosperm assemblage, measured and logged as surface exposure within the Pedro Miguel Formation, Panama Canal basin. Key lithologic intervals and units described in the text are marked to the left.

similar to the Epedeko pedotype, a pedogenically-immature successional paleosol described by Retallack and Kirby (2007). Its occurrence stratigraphically above volcaniclastic mass flow deposits further supports this interpretation. Its overlying contact with a 20-cm-thick tuff of lithological unit 3 is sharp and irregular. A carbonized tree root is preserved in life position at this contact (Fig. 3B) extending 50 cm down into lithological unit 2 and 30 cm up into lithological unit 3. The root is 7.5 cm at its widest and bifurcates downwards into unit 2. The top of the root is irregularly fractured within unit 3.

The base of lithological unit 3 is a 20-cm-thick coarse tuffaceous sandstone that grades into a 40-cm-thick, tabular, matrix-supported tuffaceous conglomerate with subrounded to rounded lapilli, each coated with an ash rind. The angiosperm leaf assemblage is found at the top of this first tuffaceous conglomerate within a ~1- to 5-cm-thick drape of tuffaceous mudstone. Leaves and preserved woody material are primarily oriented horizontally and parallel to the planar upper surface of the conglomerate (Fig. 3C). The remainder of unit 3 consists of tabular, tuffaceous conglomerates with relatively thin tuffaceous sandstone interspersed that overall grade

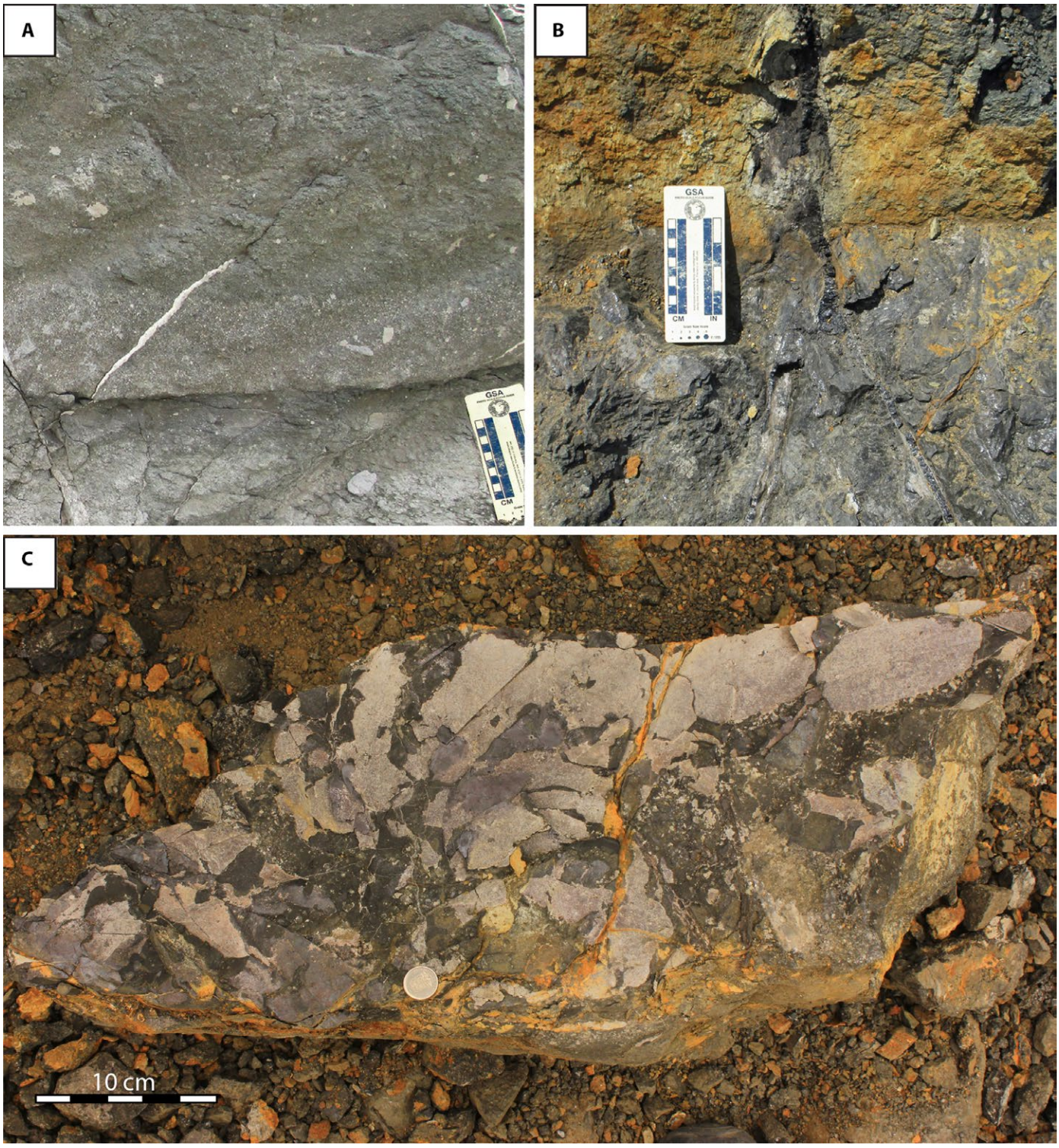

FIGURE 3. Lithological features of the Pedro Miguel Formation lithostratigraphic section. (A) Erosional base and fining upward sequence of tuffaceous sandstone to siltstone in lithological unit 1. Note the white subangular lapilli supported by matrix immediately above the erosional base. (B) Carbonized tree root in life position at contact between lithological units 2 and 3. (C) Fossil leaf assemblage within tuffaceous mudstone of lithological unit 3. Note the preserved cuticle of the leaves and the subrounded lapilli (upper left and lower right).

into the tuffaceous siltstone of lithological unit 4. These tuffaceous sandstones and conglomerates of unit 3 are interpreted as subaerial resedimented volcaniclastic debris flow deposits primarily based on the subrounded to rounded lapilli and presence of well-preserved plant fragments. The greater abundance of lapilli in this unit relative to unit 1 suggests that the original source of volcaniclastic material

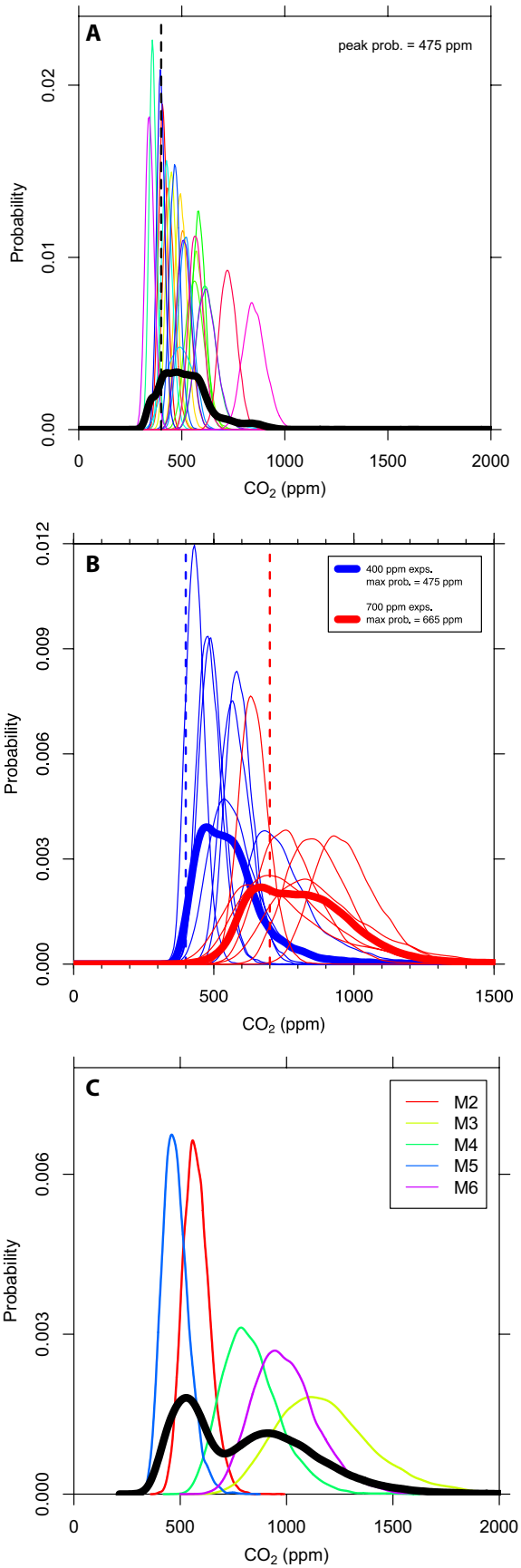

FIGURE 4. Probability density functions for the CO_2 estimates. (A) Extant rainforest leaves from the canopy. (B) Experiments at 400 and 700 ppm CO_2. (C) Miocene Pedro Miguel fossil leaves. Thin colored lines represent estimates from individual species or morphotypes (M2-M6); thick lines represent combined estimates (A–C). Vertical dashed lines in panels A and B are the known CO_2 concentrations.

was more proximal to this area during unit 3 deposition. Based on the preservation and horizontal orientation of the fossil leaves, it is unlikely that the plant material was transported far, if at all, during debris flow events. More likely, the angiosperm assemblage is the product of *in situ* leaf fall during the waning stages of a debris flow event. Overall, we interpret the angiosperm assemblage to represent an *in-situ* plant community within a volcanically disturbed coastal plain environment during the early Miocene.

Sampled floras

We collected fossil angiosperm leaves from the tuffaceous mudstone deposit interbedded between the tuffaceous conglomerates in lithological unit 3. The age of the horizon was determined by $^{238}U/^{206}Pb$ dating of detrital zircons grains taken from both tuffaceous conglomerates bracketing the leaf-bearing horizon. We analyzed 22 fossil leaves belonging to five angiosperm morphotypes (Appendix S1, see Supplemental Data with this article).

$^{238}U/^{206}Pb$ isotopic analyses were conducted at the University of Florida. Zircon grains were obtained from crushed material using standard density and magnetic separation techniques. In-situ analyses of zircon grains were performed on 20-µm spots using a Nu-Plasma multicollector plasma source mass spectrometer coupled to a 213-nm laser (LA-MC-ICP-MS). The data were acquired using the Nu-Instruments Time Resolved Analysis software. Data calibration and drift were based on multiple analyses of the reference zircon FC-1 (Black et al., 2003) repeated between every 10 ablations of the unknowns.

Leaves from extant angiosperms were collected from two different settings. The first set consists of 45 sun leaves from 21 species collected using a canopy crane in the Neotropical rainforest at Parque Nacional San Lorenzo, Panama (9.283°N, 79.966°W) (for more details, see Crifò et al., 2014). The second set consists of 80 leaves from seven species cultivated in growth chambers at 400 and 700 ppm CO_2 (for more details, see Cernusak et al., 2011).

Model for reconstructing atmospheric CO_2

We used the Franks et al. (2014) gas-exchange model to estimate atmospheric CO_2 concentration. The model is based on the relationship between the carbon assimilation rate (A_n), total leaf conductance to CO_2 ($g_{c(tot)}$), and the CO_2 concentration gradient between the atmosphere (c_a) and intercellular leaf spaces (c_i) (Farquhar and Sharkey, 1982; Von Caemmerer, 2000):

$$c_a = \frac{A_n}{g_{c(tot)} \times (1 - c_i/c_a)} \quad \text{Eq. 1}$$

This model requires measurement of stomatal density (SD, the number of stomatal pores per unit area), stomatal pore length, and single guard cell width in order to estimate $g_{c(tot)}$, and leaf and air $\delta^{13}C$

in order to estimate c_i/c_a. Stomatal measurements were made using ImageJ from digital images taken on an epifluorescence microscope (Nikon Eclipse E600; Camera Nikon DS-Ri1, Tokyo, Japan) for fossil samples and on a light microscope (Nikon Eclipse 80i; Camera Nikon DXM1200F, Tokyo, Japan) for extant samples.

Some model inputs cannot be measured directly from fossils and must be inferred from nearest living relatives, such as the photosynthetic rate at a known CO_2 concentration (A_0) and the ratio between operational and maximum stomatal conductance to CO_2 ($g_{c(op)}/g_{c(max)}$). For our Pedro Miguel fossils, we adopted the recommended values for angiosperms from Franks et al. (2014) (A_0 = 12±0.6 μmol m^{-2} s^{-1}; $g_{c(op)}/g_{c(max)}$ = 0.20±0.01; uncertainties correspond to ±1σ). It can be helpful to use inputs that are more taxon-specific (for example, at the genus or family level), but unfortunately the taxonomy of our Pedro Miguel fossils is poorly known. As a result, we also used the same "angiosperm" inputs for our 21 extant forest species in order to conservatively test their validity in Neotropical lineages. We assumed an atmospheric CO_2 $\delta^{13}C$ equal to the globally well-mixed value (–8.5‰) for the 21 forest species, and a benthic foram-constrained value of –5.7‰ for the Pedro Miguel fossils (Tipple et al., 2010). For the seven species from the CO_2 experiments, we used the values of stomatal density, carbon isotopic fractionation between leaf and air, A_0, and $g_{c(op)}$ reported by Cernusak et al. (2011); we measured stomatal pore length and guard cell width on the same leaves analyzed for leaf gas exchange by Cernusak et al. (2011).

For carbon isotope analysis, we first treated all fossils with 1N HCl to remove carbonate and then rinsed three times with distilled water. Between 0.1 and 11.0 mg of carbonate-free fossil and fresh leaf material were loaded into tin sample capsules and placed in a 50-position automated carousel on the Carlo Erba NA1500 elemental analyzer. Combustion gases were carried in a helium stream through a Conflo II interface to a Thermo Delta V Plus isotope ratio mass spectrometer. All carbon isotope results are expressed in standard delta notation relative to the Vienna PeeDee Belemnite (VPDB).

The Franks model assumes a light-saturated condition for photosynthesis. This means that sun leaves are the best candidates for the model. Because leaves entering the fossil record can be a combination of sun and shade morphotypes (e.g., Ferguson, 1985; Greenwood, 1991; Kürschner, 1997), we measured leaf vein density (D_v mm vein length / mm^2 leaf tissue; Uhl and Mosbrugger, 1999) to test for the presence of shade leaves in our fossils. D_v can scale with photosynthetic capacity (Brodribb and Feild, 2010; Sack and Scoffoni, 2013); thus, shade leaves tend to have a lower D_v than sun leaves of the same species (Crifò et al., 2014). Also, leaves living close to the forest floor—which are often shade morphotypes—assimilate more soil-derived CO_2, whose $\delta^{13}C$ value is lower than CO_2 from the well-mixed atmosphere (van der Merwe and Medina, 1989; Medina et al., 1991; Broadmeadow et al., 1992; Buchmann et al., 1997). Thus, if leaves from a single forest show a large range in $\delta^{13}C$ values (>~10‰), then the leaves with the lowest isotopic ratios probably grew near the forest floor (Graham et al., 2014).

For CO_2 reconstructions, we propagated uncertainties in all inputs with Monte Carlo simulations (10,000 resamples per species; for details, see Franks et al., 2014). We used the "density" R function to calculate probability density functions (pdfs) based on these resamples. We report c_a as the most probable CO_2 value (i.e., highest point on the pdf = mode).

RESULTS

CO_2 estimates from the present-day rainforest species range from 344 to 850 ppm, with 90% of the species ranging between 359 and 725 ppm. Combining all 21 species, the peak probability is 475 ppm (black line in Fig. 4A), which is close to the well-mixed global value of 400 ppm (Appendix S2a). CO_2 estimations from leaves in the controlled-growth chambers are also close to their target values: 475 ppm in the 400 ppm chamber and 665 ppm in the 700 ppm chamber (Fig. 4B; Appendix S2b).

Individual zircons from the tuffaceous conglomerates yielded $^{206}Pb/^{238}U$ ages ranging from ca. 60 to 18 Ma (Fig. 5A; Appendix S3). The six youngest zircons are concordant within two sigma error and give a weighted mean age of 18.01 ± 0.17 Ma, which we interpret to be the depositional age of the tuff (Fig. 5B). The older zircons include groups with early Miocene, Oligocene and Eocene ages. The

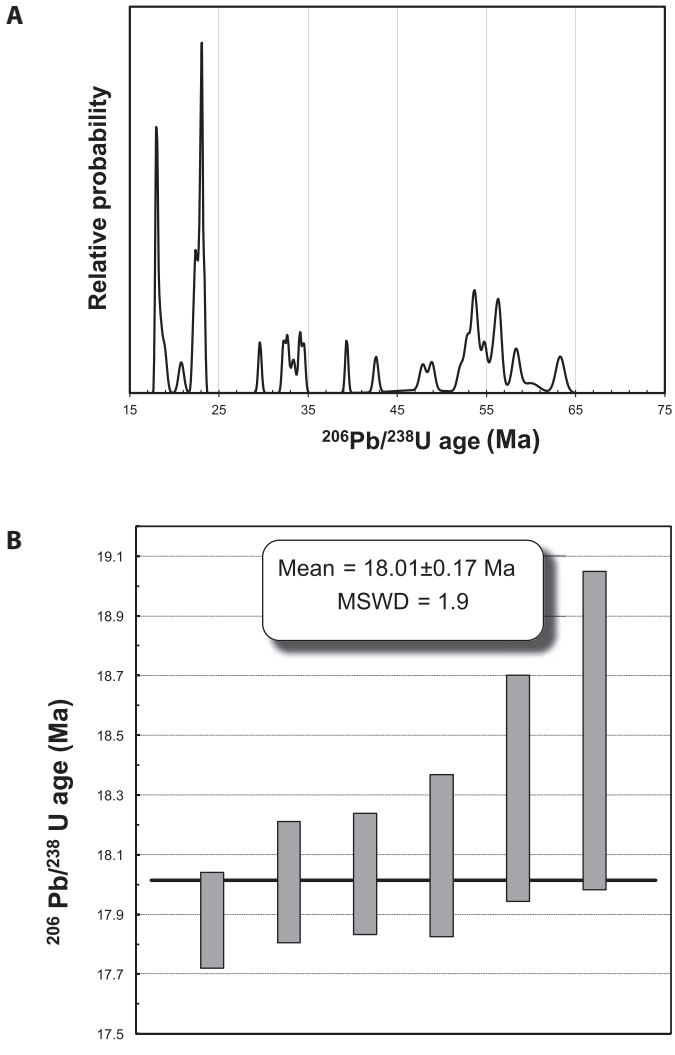

FIGURE 5. U-Pb geochronology of detrital zircon grains from Pedro Miguel Formation, Panama Canal basin. (A) Relative probability plot. (B) Weighted average plot of $^{206}Pb/^{238}U$ ages of the youngest concordant population of zircons, and mean square weighted deviation (MSWD); box heights are 2σ. The age of 18.01 ± 0.17 Ma is interpreted to be the depositional age of the tuff.

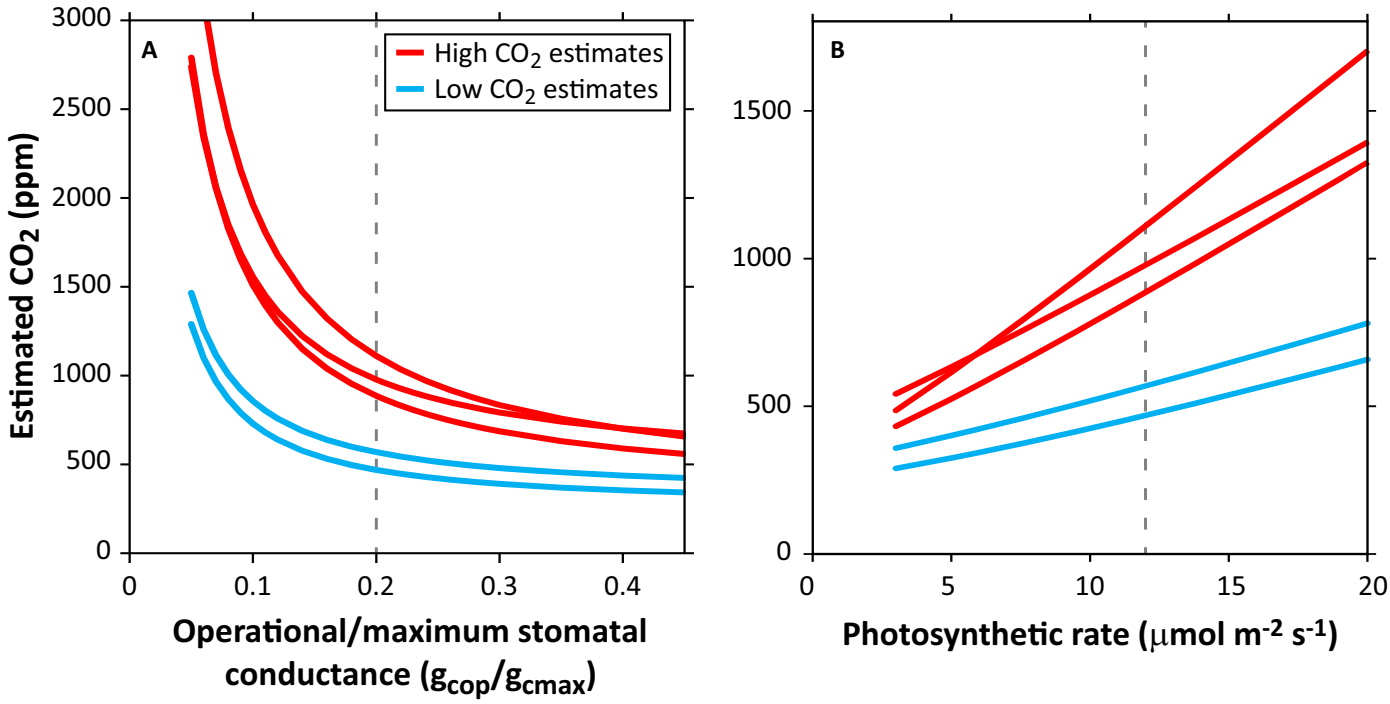

FIGURE 6. Sensitivity of estimated CO_2 in the five fossil morphotypes to changes in (A) the ratio between operational and maximum stomatal conductance to CO_2 and (B) leaf photosynthetic rate at 360 ppm CO_2. In both panels, the red and blue curves are associated with the morphotypes that estimate higher and lower CO_2, respectively (see Fig. 4C). The vertical dashed lines are input values used in the standard model runs (e.g., Fig. 4C).

age spectrum of the detrital zircons is typical of strata within the Panama Canal basin and elsewhere in central Panama (Ramírez et al., 2016).

D_v in the five fossil morphotypes varied from 6.9 to 12.9 mm of vein length per mm² of leaf tissue. Leaf $\delta^{13}C$ mean values of the morphotypes have a range of 3.2‰, from –30.2 to –27.0‰ (Appendix S2c).

CO_2 estimates of the five morphotypes from the Pedro Miguel flora show a bimodal distribution, with two species suggesting lower CO_2 and three species higher CO_2 (Fig. 4C). In the combined probability, the first mode is at 528 ppm and the second at 912 ppm (black line in Fig. 4C; Appendix S2c); 95% of the resampled estimates exceed 436 ppm.

DISCUSSION

Application of the Franks et al. (2014) method to living vegetation, both in a natural rainforest and in greenhouse experiments at current and elevated CO_2, indicates that overall the method does well at estimating CO_2, although estimates for individual estimates vary by over two-fold. This underscores the importance of using multiple species when applying the proxy.

The generally accurate estimates from the 21 tree forest species is particularly noteworthy given that for inputs like A_0 and $g_{c(op)}/g_{c(max)}$ we used the generic values for angiosperms recommended by Franks et al. (2014) instead of taxon-specific values. This is an important check on the model, increasing confidence that it is reliable with Neotropical vegetation at elevated CO_2, and a positive aspect for studies that wish to apply the model to Neotropical angiosperm fossils where taxonomic affinities are uncertain.

We explored whether taxon-specific values of A_0 for 16 of the 21-canopy species would lead to more accurate estimates. These A_0 measurements were made on a different set of leaves than the morphology and isotopic measurements, but come from the same forest (Appendix S4). Overall, CO_2 estimates for these species (median = 450 ppm) are not much different than the original estimates (median = 421 ppm). This implies that the scatter in Figure 4A is not due to an incorrect parameterization of A_0.

The bimodality of the Miocene CO_2 estimates requires scrutiny (Fig. 4C). Of the fossil inputs that were not directly measured, variations in A_0 and $g_{c(op)}/g_{c(max)}$ have the greatest effect on estimated CO_2 (Maxbauer et al., 2014). Franks et al. (2014) recommend an A_0 value of 12 mol m^{-2} s^{-1} for angiosperms grown at 360 ppm CO_2. If A_0 is reduced to ~5 μmol m^{-2} s^{-1} for the three "high-CO_2" fossil morphotypes, the downward revised CO_2 estimates converge with the two "low-CO_2" morphotypes (Fig. 6B). However, we consider this scenario unlikely because both the D_v and $\delta^{13}C$ values of all fossil samples lie within a range that closely match the observed values of extant upper-canopy leaves (Crifò et al., 2014; Graham et al., 2014). D_v is known as an important regulator of A_0 among species of multiple functional plant groups (Brodribb et al., 2007; Boyce et al., 2009). By facilitating water transport, the high D_v of our fossil leaves should have led to high gas exchange, leading to a high A_0 (Hubbard et al., 2001; Brodribb et al., 2007; Brodribb and Feild, 2010). The combination of a sun habit and a photosynthetic rate of ~5 μmol m^{-2} s^{-1} for Neotropical angiosperm leaves today is unusual (Oberbauer and Strain, 1984; Chazdon et al., 1996; Zotz and Winter, 1996; Kitajima et al., 1997). Alternatively, convergence in the fossil CO_2 estimates can be achieved by increasing A_0 in the two low-CO_2 morphotypes to ~30 μmol m^{-2} s^{-1}. Such values are near the limit observed today in tropical canopy trees (Kitajima et al., 1997).

Our paleo-CO_2 estimates assume a $g_{c(op)}/g_{c(max)}$ of 0.20. This value is close to the across-species mean reported by Franks et al. (2014) and (McElwain et al., 2016) (0.23), but individual species range between 0.06 and 0.44. In our experimental treatments, measured $g_{c(op)}/g_{c(max)}$ values were mostly on the lower end of this range (mean = 0.10; range = 0.01-0.35; Appendix S5). We also observed a small but significant CO_2 effect on $g_{c(op)}/g_{c(max)}$ (species means of 0.12 and 0.08 for 400 ppm and 700 ppm-grown plants, respectively; Appendix S6). If we reduce $g_{c(op)}/g_{c(max)}$ in the low-CO_2 fossil morphotypes to ~0.05, the revised CO_2 estimates increase and converge with the high CO_2 estimates (Fig. 6A). Assuming a higher $g_{c(op)}/g_{c(max)}$ value for the high-CO_2 morphotypes will decrease their estimated CO_2, but not enough to converge their values with the low-CO_2 morphotypes. The low number of fossil species may also partly explain the bimodality. If we artificially degrade our extant canopy data set to five species, a bimodal pattern in estimated CO_2 is common (Appendix S7).

We conclude from the sensitivity analysis that the most plausible adjustments to our inputs are to either decrease $g_{c(op)}/g_{c(max)}$ or increase A_0 in the two "low CO_2" morphotypes, or some combination of the two. Thus, we put greater confidence in the high CO_2 mode shown in Figure 2C. Independent of these arguments, we consider it highly likely (with 95% confidence) that CO_2 exceeded 436 ppm. This is important because existing CO_2 estimates from ~18 Ma generally are <450 ppm (Fig. 1B), a challenging scenario that is seemingly at odds with the warmer global temperatures that characterized the early and middle Miocene (Zhang et al., 2013; Goldner et al., 2014). If CO_2 exceeded 450 ppm, climate simulations become far easier to reconcile with the proxy indicators of warmth during this period.

ACKNOWLEDGEMENTS

This work was supported by the Smithsonian Tropical Research Institute, Autoridad del Canal de Panama (ACP), the Mark Tupper Fellowship, Ricardo Perez S.A, National Science Foundation grant EAR 0824299 and OISE, EAR, DRL 0966884, the Anders Foundation, Gregory D. and Jennifer Walston Johnson and 1923 Fund. We also thank Klaus Winter, Joseph Wright, Louis Santiago, Camila Crifò, Andres Baresh and Carrie Tribble for helpful discussions, and the anonymous reviewers for helpful comments.

SUPPORTING INFORMATION

Additional Supporting Information may be found online in the supporting information tab for this article.

LITERATURE CITED

Badger, M. P., D. N. Schmidt, A. Mackensen, and R. D. Pancost. 2013a. High-resolution alkenone palaeobarometry indicates relatively stable pCO_2 during the Pliocene (3.3-2.8 Ma). *Philos Trans A Math Phys Eng Sci* 371. https://doi.org/10.1098/rsta.2013.0094.

Badger, M. P. S., C. H. Lear, R. D. Pancost, G. L. Foster, T. R. Bailey, M. J. Leng, and H. A. Abels. 2013b. CO_2 drawdown following the middle Miocene expansion of the Antarctic Ice Sheet. *Paleoceanography* 28: 42–53.

Barclay, R. S., and S. L. Wing. 2016. Improving the Ginkgo CO_2 barometer: Implications for the early Cenozoic atmosphere. *Earth and Planetary Science Letters* 439: 158–171.

Beerling, D. J., and D. L. Royer. 2011. Convergent Cenozoic CO_2 history. *Nature Geosci* 4: 418–420.

Beerling, D. J., A. Fox, and C. W. Anderson. 2009. Quantitative uncertainty analyses of ancient atmospheric CO_2 estimates from fossil leaves. *American Journal of Science* 309: 775–787.

Black, L. P., S. L. Kamo, I. S. Williams, R. Mundil, D. W. Davis, R. J. Korsch, and C. Foudoulis. 2003. The application of SHRIMP to Phanerozoic geochronology; a critical appraisal of four zircon standards. *Chemical Geology* 200: 171–188.

Boyce, C. K., T. J. Brodribb, T. S. Feild, and M. A. Zwieniecki. 2009. Angiosperm leaf vein evolution was physiologically and environmentally transformative. *Proceedings of the Royal Society B: Biological Sciences* 276: 1771–1776.

Bradshaw, C. D., D. J. Lunt, R. Flecker, and T. Davies-Barnard. 2015. Disentangling the roles of late Miocene palaeogeography and vegetation – Implications for climate sensitivity. *Palaeogeography, Palaeoclimatology, Palaeoecology* 417: 17–34.

Breecker, D. O., and G. J. Retallack. 2014. Refining the pedogenic carbonate atmospheric CO2 proxy and application to Miocene CO_2. *Palaeogeography, Palaeoclimatology, Palaeoecology* 406: 1–8.

Broadmeadow, M. S. J., H. Griffiths, C. Maxwell, and A. M. Borland. 1992. The carbon isotope ratio of plant organic material reflects temporal and spatial variations in CO_2 within tropical forest formations in Trinidad. *Oecologia* 89: 435–441.

Brodribb, T. J., and T. S. Feild. 2010. Leaf hydraulic evolution led a surge in leaf photosynthetic capacity during early angiosperm diversification. *Ecology Letters* 13: 175–183.

Brodribb, T. J., T. S. Feild, and G. J. Jordan. 2007. Leaf maximum photosynthetic rate and venation are linked by hydraulics. *Plant Physiology* 144: 1890–1898.

Buchmann, N., W.-Y. Kao, and J. Ehleringer. 1997. Influence of stand structure on carbon-13 of vegetation, soils, and canopy air within deciduous and evergreen forests in Utah, United States. *Oecologia* 110: 109–119.

Cernusak, L. A., K. Winter, C. Martínez, E. Correa, J. Aranda, M. Garcia, C. Jaramillo, and B. L. Turner. 2011. Responses of Legume Versus Nonlegume Tropical Tree Seedlings to Elevated CO2 Concentration. *Plant Physiology* 157: 372–385.

Chazdon, R. L., R. W. Pearcy, D. W. Lee, and N. Fetcher. 1996. Photosynthetic Responses of Tropical Forest Plants to Contrasting Light Environments. *In* S. S. Mulkey, R. L. Chazdon, and A. P. Smith [eds.], Tropical Forest Plant Ecophysiology 10.1007/978-1-4613-1163-8_1 10.1007/978-1-4613-1163-8_1, 5–55. Springer US, Boston, MA.

Crifò, C., E. D. Currano, A. Baresch, and C. Jaramillo. 2014. Variations in angiosperm leaf vein density have implications for interpreting life form in the fossil record. *Geology* 42: 919–922.

Ekart, D. D., T. E. Cerling, I. P. Montanez, and N. J. Tabor. 1999. A 400 million year carbon isotope record of pedogenic carbonate; implications for paleoatomospheric carbon dioxide. *American Journal of Science* 299: 805–827.

Farquhar, G. D., and T. D. Sharkey. 1982. Stomatal conductance and photosynthesis. *Annual review of plant physiology* 33: 317–345.

Ferguson, D. K. 1985. The origin of leaf-assemblages—new light on an old problem. *Review of Palaeobotany and Palynology* 46: 117–188.

Foster, G. L., C. H. Lear, and J. W. B. Rae. 2012. The evolution of pCO_2, ice volume and climate during the middle Miocene. *Earth and Planetary Science Letters* 341: 243–254.

Franks, P. J., D. L. Royer, D. J. Beerling, P. K. Van de Water, D. J. Cantrill, M. M. Barbour, and J. A. Berry. 2014. New constraints on atmospheric CO_2 concentration for the Phanerozoic. *Geophysical Research Letters* 41: 4685–4694.

Goldner, A., N. Herold, and M. Huber. 2014. The challenge of simulating the warmth of the mid-Miocene climatic optimum in CESM1. *Climate of the Past* 10: 523–536.

Graham, H. V., M. E. Patzkowsky, S. L. Wing, G. G. Parker, M. L. Fogel, and K. H. Freeman. 2014. Isotopic characteristics of canopies in simulated leaf assemblages. *Geochimica et Cosmochimica Acta* 144: 82–95.

Greenop, R., G. L. Foster, P. A. Wilson, and C. H. Lear. 2014. Middle Miocene climate instability associated with high-amplitude CO_2 variability. *Paleoceanography* 29: 845–853.

Greenwood, D. R. 1991. The taphonomy of plant macrofossils. *In* The Processes of Fossilization, pp 141–169. Columbia University Press.

Grein, M., C. Oehm, W. Konrad, T. Utescher, L. Kunzmann, and A. Roth-Nebelsick. 2013. Atmospheric CO_2 from the late Oligocene to early Miocene based on photosynthesis data and fossil leaf characteristics. *Palaeogeography, Palaeoclimatology, Palaeoecology* 374: 41–51.

Hansen, J., M. Sato, G. Russell, and P. Kharecha. 2013. Climate sensitivity, sea level and atmospheric carbon dioxide. *Philosophical Transactions of the Royal Society A: Mathematical, Physical and Engineering Sciences* 371: 20120294.

Hubbard, R. M., M. G. Ryan, V. Stiller, and J. S. Sperry. 2001. Stomatal conductance and photosynthesis vary linearly with plant hydraulic conductance in ponderosa pine. *Plant, Cell & Environment* 24: 113–121.

Kitajima, K., S. S. Mulkey, and S. J. Wright. 1997. Seasonal leaf phenotypes in the canopy of a tropical dry forest: photosynthetic characteristics and associated traits. *Oecologia* 109: 490–498.

Knorr, G., M. Butzin, A. Micheels, and G. Lohmann. 2011. A warm Miocene climate at low atmospheric CO2 levels. *Geophysical Research Letters* 38.

Kürschner, W. M. 1997. The anatomical diversity of recent and fossil leaves of the durmast oak (Quercus petraea Lieblein/Q. pseudocastanea Goeppert) — implications for their use as biosensors of palaeoatmospheric CO_2 levels. *Review of Palaeobotany and Palynology* 96: 1–30.

Kürschner, W. M., Z. Kvaček, and D. L. Dilcher. 2008. The impact of Miocene atmospheric carbon dioxide fluctuations on climate and the evolution of terrestrial ecosystems. *Proceedings of the National Academy of Sciences* 105: 449–453.

MacFadden, B. J., J. I. Bloch, H. Evans, D. A. Foster, G. S. Morgan, A. Rincon, and A. R. Wood. 2014. Temporal Calibration and Biochronology of the Centenario Fauna, Early Miocene of Panama. *The Journal of Geology* 122: 113–135.

Maxbauer, D. P., D. L. Royer, and B. A. LePage. 2014. High Arctic forests during the middle Eocene supported by moderate levels of atmospheric CO_2. *Geology* 42: 1027–1030.

McElwain, J. C., C. Yiotis, and T. Lawson. 2016. Using modern plant trait relationships between observed and theoretical maximum stomatal conductance and vein density to examine patterns of plant macroevolution. *New Phytologist* 209: 94–103.

Medina, E., L. Sternberg, and E. Cuevas. 1991. Vertical stratification of d13C values in closed natural and plantation forests in the Luquillo mountaints, Puerto Rico. *Oecologia* 87: 369–372.

Mejía, L. M., A. Méndez-Vicente, L. Abrevaya, K. T. Lawrence, C. Ladlow, C. Bolton, I. Cacho, and H. Stoll. 2017. A diatom record of CO_2 decline since the late Miocene. *Earth and Planetary Science Letters* 479: 18–33.

van der Merwe, N. J., and E. Medina. 1989. Photosynthesis and 13C12C ratios in Amazonian rain forests. *Geochimica et Cosmochimica Acta* 53: 1091–1094.

Montes, C., A. Cardona, R. McFadden, S. E. Morón, C. A. Silva, S. Restrepo-Moreno, D. A. Ramírez, et al. 2012. Evidence for middle Eocene and younger land emergence in central Panama: Implications for Isthmus closure. *Geological Society of America Bulletin* 124: 780–799.

Oberbauer, S. F., and B. R. Strain. 1984. Photosynthesis and successional status of Costa Rican rain forest trees. *Photosynthesis Research* 5: 227–232.

Quade, J., and T. E. Cerling. 1995. Expansion of C_4 grasses in the Late Miocene of Northern Pakistan: evidence from stable isotopes in paleosols. *Palaeogeography, Palaeoclimatology, Palaeoecology* 115: 91–116.

Ramírez, D. A., D. A. Foster, K. Min, C. Montes, A. Cardona, and G. Sadove. 2016. Exhumation of the Panama basement complex and basins: Implications for the closure of the Central American seaway. *Geochemistry, Geophysics, Geosystems* 17: 1758–1777.

Reichgelt, T., W. J. D'Andrea, and B. R. S. Fox. 2016. Abrupt plant physiological changes in southern New Zealand at the termination of the Mi-1 event reflect shifts in hydroclimate and pCO_2. *Earth and Planetary Science Letters* 455: 115–124.

Retallack, G. J. 2009. Refining a pedogenic-carbonate CO_2 paleobarometer to quantify a middle Miocene greenhouse spike. *Palaeogeography, Palaeoclimatology, Palaeoecology* 281: 57–65.

Retallack, G. J., and M. X. Kirby. 2007. Middle Miocene global change and paleogeography of Panama. *Palaios* 22: 667–679.

Roth-Nebelsick, A., T. Utescher, V. Mosbrugger, L. Diester-Haass, and H. Walther. 2004. Changes in atmospheric CO_2 concentrations and climate from the Late Eocene to Early Miocene: palaeobotanical reconstruction based on fossil floras from Saxony, Germany. *Palaeogeography, Palaeoclimatology, Palaeoecology* 205: 43–67.

Royer, D. L. 2014. 6.11 - Atmospheric CO_2 and O_2 During the Phanerozoic: Tools, Patterns, and Impacts A2 - Holland, Heinrich D. *In* K. K. Turekian [ed.], Treatise on Geochemistry (Second Edition), 251–267. Elsevier, Oxford.

Royer, D. L., S. L. Wing, D. J. Beerling, D. W. Jolley, P. L. Koch, L. J. Hickey, and R. A. Berner. 2001. Paleobotanical Evidence for Near Present-Day Levels of Atmospheric CO_2 During Part of the Tertiary. *Science* 292: 2310–2313.

Sack, L., and C. Scoffoni. 2013. Leaf venation: structure, function, development, evolution, ecology and applications in the past, present and future. *New Phytologist* 198: 983–1000.

Steinthorsdottir, M., V. Vajda, and M. Pole. 2018. Significant transient pCO_2 perturbation at the New Zealand Oligocene-Miocene transition recorded by fossil plant stomata. *Palaeogeography, Palaeoclimatology, Palaeoecology* (in press). https://doi.org/10.1016/j.palaeo.2018.01.039.

Super, J. R., E. Thomas, M. Pagani, M. Huber, C. O'Brien, and P. M. Hull. 2018. North Atlantic temperature and pCO_2 coupling in the early-middle Miocene. *Geology* 46: 519–522.

Tesfamichael, T., B. Jacobs, N. Tabor, L. Michel, E. Currano, M. Feseha, R. Barclay, et al. 2017. Settling the issue of "decoupling" between atmospheric carbon dioxide and global temperature: $[CO_2]$atm reconstructions across the warming Paleogene-Neogene divide. *Geology* 45: 999–1002.

Tipple, B. J., S. R. Meyers, and M. Pagani. 2010. Carbon isotope ratio of Cenozoic CO_2: A comparative evaluation of available geochemical proxies. *Paleoceanography* 25: 3202.

Uhl, D., and V. Mosbrugger. 1999. Leaf venation density as a climate and environmental proxy: a critical review and new data. *Palaeogeography, Palaeoclimatology, Palaeoecology* 149: 15–26.

Von Caemmerer, S. 2000. Biochemical models of leaf photosynthesis. Csiro Publishing.

Wang, Y., A. Momohara, L. Wang, J. Lebreton-Anberrée, and Z. Zhou. 2015. Evolutionary history of atmospheric CO_2 during the Late Cenozoic from fossilized metasequoia needles. *PLoS ONE* 10: e0130941.

Zachos, J. C., G. R. Dickens, and R. E. Zeebe. 2008. An early Cenozoic perspective on greenhouse warming and carbon-cycle dynamics. *Nature* 451: 279–283.

Zhang, Y. G., M. Pagani, Z. Liu, S. M. Bohaty, and R. DeConto. 2013. A 40-million-year history of atmospheric CO_2. *Phil. Trans. R. Soc. A* 371: 20130096.

Zotz, G., and K. Winter. 1996. Seasonal Changes in Daytime Versus Nighttime CO_2 Fixation of Clusia uvitana In Situ. *In* K. Winter and J. A. C. Smith [eds.], Crassulacean Acid Metabolism: Biochemistry, Ecophysiology and Evolution, 312–323. Springer Berlin Heidelberg, Berlin, Heidelberg.